

Molecular Hydrogen Line Emission from the Reflection Nebula Parsamyan 18

S. D. Ryder^{*}, L. E. Allen, M. G. Burton, M. C. B. Ashley and J. W. V. Storey

School of Physics, University of New South Wales, Sydney 2052, Australia

Accepted 1997 September 15. Received August 7; in original form 1997 June 5

ABSTRACT

The newly-commissioned University of New South Wales Infrared Fabry-Perot (UNSWIRF) has been used to image molecular hydrogen emission at 2.12 and 2.25 μm in the reflection nebula Parsamyan 18. P 18 is known to exhibit low values of the $(1-0)/(2-1)$ $S(1)$ ratio suggestive of UV-pumped fluorescence rather than thermal excitation by shocks. Our line ratio mapping reveals the full extent of this fluorescent emission from extended arc-like features, as well as a more concentrated thermal component in regions closer to the central exciting star. We show that the emission morphology, line fluxes, and gas density are consistent with the predictions of photodissociation region (PDR) theory. Those regions with the highest intrinsic $1-0$ $S(1)$ intensities also tend to show the highest $(1-0)/(2-1)$ $S(1)$ line ratios. Furthermore, variations in the line ratio can be attributed to intrinsic fluctuations in the incident radiation field and/or the gas density, through the self-shielding action of H_2 . An isolated knot of emission discovered just outside P 18, and having both an unusually high $(1-0)/(2-1)$ $S(1)$ ratio and relative velocity provides additional evidence for an outflow source associated with P 18.

Key words: reflection nebulae – ISM: individual: Parsamyan 18 – shock waves – molecular processes

1 INTRODUCTION

The ‘cometary nebula’ Parsamyan 18 (P 18 = NGC 2316 = L 1654) has properties characteristic of both reflection and emission nebulae. Near-infrared emission lines of molecular hydrogen have been observed, as well as emission features at 3.3, 6.2, 7.7, 8.6, and 11.3 μm (Sellgren 1986; Burton et al. 1990; Sellgren, Werner, & Allamandola 1996) attributed to aromatic hydrocarbons. Similar emission features and near-infrared colours were found in over half of the visual reflection nebulae surveyed by Sellgren et al. (1996). López et al. (1988) used a combination of optical, infrared, and radio continuum observations to argue that the two brightest regions of P 18 are not in fact stars, but actually represent light from a heavily-obscured H II region breaking through a dust shell surrounding the exciting early B-type star. On the basis of (unpublished) optical spectra however, Sellgren et al. (1996) list both components as being stellar, with the north-eastern star (Star ‘A’, a B2-3e star with $V = 13.21$) illuminating the dust as well as exciting the atomic and molecular hydrogen.

P 18 was only the second object (after NGC 2023; Gatley et al. 1987) found to have infrared H_2 emission line ratios similar to the predictions of UV-pumped fluorescence, rather than thermal excitation by shocks (Sellgren 1986). In nearly all such studies to date, line ratios and inferred excitation mechanisms are based on large-aperture spectra, or from only a single pointing. With the advent of imaging infrared Fabry-Perot systems (with resolving powers $R \gtrsim 1000$ that provide the necessary contrast between line and continuum), it has now become possible to carry out line ratio *mapping*. This could be a useful aid in discriminating between the sources of excitation, on the basis of line ratio trends and morphology. In this paper, we report the results of our H_2 line imaging of P 18 using the University of New South Wales Infrared Fabry-Perot (UNSWIRF).

Our results show that ‘collisional fluorescence’ is occurring in P 18. That is, pure fluorescent line ratios are thermally modified by the effects of collisions. This occurs in dense molecular clouds where H_2 self-shielding maintains a significant column density of the molecule close to the cloud surface (*i.e.*, $A_V < 1$), where the gas temperature can reach a few thousand degrees (*e.g.*, Sternberg & Dalgarno 1989; Burton, Hollenbach, & Tielens 1990 [hereafter BHT]). Emission line ratios are then sensitive to the density and radiation

^{*} Present address: Joint Astronomy Centre, 660 N. A’Ohoku Place, Hilo, HI 96720, U.S.A. E-mail: sryder@jach.hawaii.edu.

field, and so observations with sufficiently high spatial resolution can be used to trace the variation of these parameters within a source. Large aperture measurements of both H_2 and high- J CO lines (*e.g.*, Hayashi et al. 1985; Stutzki et al. 1990) of many such ‘photodissociation regions’ or PDRs (Tielens & Hollenbach 1985; BHT) have indicated they are clumpy, containing regions where the density must be ten to a hundred times greater than the surrounding cloud. High spatial resolution H_2 line ratio measurements may now be used to probe how this high density gas is distributed.

2 OBSERVATIONS

UNSWIRF is a 70 mm diameter Queensgate (UK) Ltd. etalon with $R \sim 4000$, tunable over both the H and K windows (Ryder et al. 1997). When used in conjunction with the wide-field mode of IRIS[†] at the $f/36$ focus of the Anglo-Australian Telescope, a (roughly circular) field of 1.7 arcmin diameter at $0.77 \text{ arcsec pixel}^{-1}$ is produced. Appropriate 1 per cent bandpass filters are used to ensure only a single order is passed by the etalon.

Observations of P 18 in the $H_2 1 - 0 S(1)$ ($2.122 \mu\text{m}$) and $H_2 2 - 1 S(1)$ ($2.248 \mu\text{m}$) lines were obtained on 1996 April 4 UT. A sequence of four images spanning the peak of the $2.122 \mu\text{m}$ line (as determined from observations of OMC-1) and separated by $\sim 2/3$ of the instrumental profile width were obtained with UNSWIRF, while for the $2.248 \mu\text{m}$ line, just three images spaced $\sim 1/2$ of the profile width apart were taken. In each case, another image at 3–4 profile widths from the line centre was obtained in order to sample the continuum. An integration time of 120 s per etalon setting was used, with non-destructive readouts every 5 s. The same exposure sequence was carried out on the sky 5 arcmin east of P 18. The object and sky exposures were repeated (with slight offsets from the previous positions), leading to total on-source integration times of 1920 s and 2880 s in the 2.122 and $2.248 \mu\text{m}$ lines, respectively.

Dark current subtraction and linearisation are performed during readout. The object frames were sky-subtracted, and then flatfielded using normalised dome flat-fields, using in each case images at the matching etalon settings. All frames were first registered using field stars, and all frames at a given etalon setting were averaged together. The continuum frames, appropriately scaled, were then subtracted from all other images to leave just pure line emission in each.

At this stage, the emission line images were ‘stacked’ into cubes of increasing etalon spacing / wavelength, so that a Lorentzian profile could be fitted to the (3 or 4) point spectrum at each pixel. Having already fixed the continuum level to be zero, the number of free parameters in the fitting was further reduced by constraining the width of the profile to be the same as that found by fits to high-resolution scans of Krypton arc lines ($2.1165 \mu\text{m}$ and $2.2485 \mu\text{m}$ for the $2.12 \mu\text{m}$ and $2.25 \mu\text{m}$ cubes, respectively). We justify this on the basis that the narrow H_2 line widths ($16\text{--}20 \text{ km s}^{-1}$) observed

[†] The Infrared Imager and Spectrometer (Allen et al. 1993) uses a 128×128 HgCdTe array manufactured by Rockwell International Science Centre, CA.

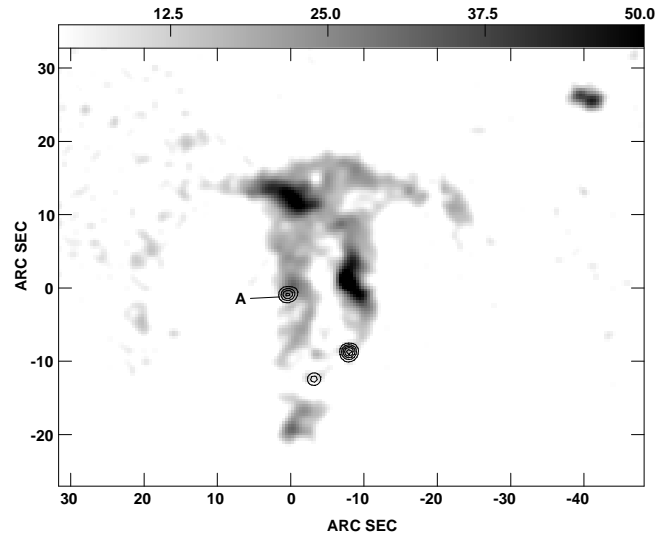


Figure 1. Grey-scale image of the $H_2 1 - 0 S(1)$ ($2.122 \mu\text{m}$) emission line intensity in P 18, with contours of the $2.12 \mu\text{m}$ continuum sources overlaid. The continuum source identified previously as star ‘A’, and assumed to be the source of excitation of the H_2 , is marked. The coordinate system shown is in arcseconds north and east of star ‘A’, which has coordinates of $06^{\text{h}}59^{\text{m}}41^{\text{s}}.6$, $-07^{\circ}46'29''$ (J2000). The grey scale-wedge indicates flux densities in units of $10^{-16} \text{ ergs cm}^{-2} \text{ s}^{-1} \text{ arcsec}^{-2}$. The 0.77 arcsec pixels have been re-sampled onto a finer grid, then smoothed with a 1 arcsec Gaussian to accentuate the overlapping arc features mentioned in the text. The increased noise in the northeast quadrant is due to a defect in one of the etalon anti-reflection coatings.

in P 18 by Burton et al. (1990) would not be resolvable by UNSWIRF ($\text{FWHM} \sim 65 \text{ km s}^{-1}$ at $2.12 \mu\text{m}$). The output of the line fitting includes maps of the peak intensity, as well as the etalon setting corresponding to that peak. Blanking masks are constructed by requiring that the fitted peak position must lie within the range covered by the etalon sequence. Flux calibration, and continuum scaling factors, are provided by photometry of $10 \times 1 \text{ s}$ observations of the spectroscopic standard BS 2882 ($K = 5.18$), also at the same etalon settings used for P 18.

3 RESULTS

Figure 1 shows a grey-scale map of the $2.12 \mu\text{m}$ line intensity, with contours of the three brightest $2.12 \mu\text{m}$ continuum sources superimposed (including star ‘A’) to aid in comparing our new data to that elsewhere in the literature (*e.g.*, López et al. 1988). The H_2 emission structure can be conveniently divided into a number of distinct regions, as outlined in Figure 2. The emission line fluxes of each region are tabulated in Table 1. The integrated emission line flux of P 18 measured from the $2.12 \mu\text{m}$ image is $(13.1 \pm 0.6) \times 10^{-13} \text{ ergs cm}^{-2} \text{ s}^{-1}$, compared with the $(4.5 \pm 0.3) \times 10^{-13} \text{ ergs cm}^{-2} \text{ s}^{-1}$ found in the matching $2.25 \mu\text{m}$ image. Uncertainties in the absolute flux calibration and line-fitting procedures are roughly comparable in magnitude with the noise contribution ($\sim 1.8 \times 10^{-16} \text{ ergs cm}^{-2} \text{ s}^{-1}$) per pixel over which the emission is summed.

The morphology of the infrared molecular hydrogen emission differs somewhat from the ‘cometary’ nature dis-

Table 1. H₂ Line Intensities, Ratios and Velocities in P 18

Region ^a	d ^b (arcsec)	FUV Field ^c (G ₀)	1 – 0 S(1) Flux (ergs cm ⁻² s ⁻¹)	2 – 1 S(1) Flux (ergs cm ⁻² s ⁻¹)	N ^d	Ratio	Peak (1 – 0) S(1) Flux in region (ergs cm ⁻² s ⁻¹ arcsec ⁻²)	Ratio at Peak	Relative Velocity ^e (km s ⁻¹)
Whole Source	13.1 ± 0.6(-13)	4.5 ± 0.3(-13)	2147	2.9 ± 0.4
1 (E Arc)	22	2400	2.7 ± 0.1(-13)	1.1 ± 0.1(-13)	766	2.4 ± 0.3	1.7(-15)	1.6	+8
2 (N Peak)	15	5060	2.2 ± 0.1(-13)	8.1 ± 0.5(-14)	248	2.7 ± 0.3	5.5(-15)	2.9	+2
3 (Central Arc)	1.9 ± 0.1(-13)	4.9 ± 0.4(-14)	260	3.9 ± 0.5	3.1(-15)	4.8	0
4 (S Peak)	18	3500	8.5 ± 0.5(-14)	3.3 ± 0.3(-14)	147	2.6 ± 0.4	3.1(-15)	3.3	-2
5 (W Peak)	8	17800	3.0 ± 0.1(-13)	8.3 ± 0.6(-14)	373	3.6 ± 0.4	7.9(-15)	7.0	-1
6 (NW Arc)	19	3200	1.1 ± 0.1(-13)	4.6 ± 0.3(-14)	141	2.5 ± 0.3	2.5(-15)	2.9	+4
7 (W Arc)	25	1800	9.7 ± 0.5(-14)	4.0 ± 0.3(-14)	172	2.4 ± 0.3	2.0(-15)	2.4	-3
8 (P 18-NW) ^f	48	500	3.8 ± 0.2(-14)	4.4 ± 1.2(-15)	40	8.6 ± 2.9	4.9(-15)	13.7	+14

^aNumbering as in Figure 2.

^bProjected distance from Star A.

^cIn units of the average interstellar field, for the projected distance from Star A.

^dNumber of pixels, of size 0.77'' × 0.77'', included in region.

^eRelative velocity of H₂ emission from region.

^fThis region is not linked with the others and is probably shock-excited, rather than irradiated by Star A (Section 4.4).

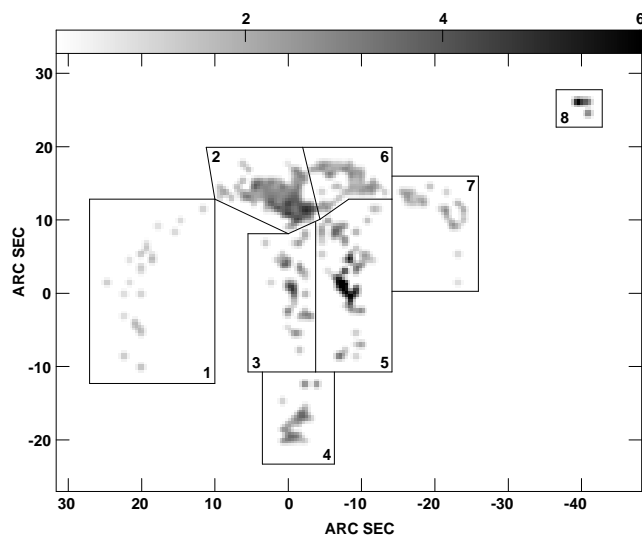


Figure 2. Grey-scale image of the H₂ 1 – 0 S(1)/2 – 1 S(1) ratio in P 18, for all points in which a reliable detection (S/N > 3) at 2.25 μm was achieved. The numbered polygons outline the eight separate emission regions in and around P 18, as given in Table 1. As in Figure 1, the 0.77 arcsec pixels have been re-sampled onto a finer grid, but no smoothing has been applied.

played in the optical (Cohen 1974), and from the broad-band infrared and radio continuum images of López et al. (1988). Instead of a cone, the appearance is one of two incomplete, but overlapping arcs. With reference to Figure 2, one arc is outlined by the contiguous regions (1, 2, 5, 4), while the other is defined by the regions (4, 3, 6, 7). Each arc, if it were part of a complete ring, would have a diameter of ~ 30 arcsec, or 0.16 pc, assuming P 18 to be 1.1 kpc away (Hilton & Lahulla 1995). Star ‘A’, assumed to be the exciting source, sits on the periphery of the arc that extends to the west, and halfway between the centre and the edge of the easterly arc. The emission peaks (in both the 2.12 μm and the 2.25 μm images) in the areas due north and south of star

‘A’, where these two arcs overlap. In addition, more prominent emission at 2.12 μm is found on the western edge of the eastern arc, ~ 8 arcsec due west of star ‘A’, as well as in an isolated knot of emission some 50 arcsec to the northwest of star ‘A’. This isolated patch (hereafter designated P 18-NW) has no continuum counterpart or obvious exciting source. Although none of this emission-line structure is apparent in the K-band image of López et al. (1988), it is faintly visible in the FITS version of the K’ imaging survey of CO molecular outflow sources carried out by Hodapp (1994).

Figure 2 is a grey-scale image of the (1 – 0)/(2 – 1) ratio in P 18 for all points in which the 2 – 1 intensity could be determined. The values found range from 1 – 2 in the eastern arc, to as much as 7 in the nebular arc just west of Star ‘A’, and even higher in P 18-NW (though the 2 – 1 detection here is barely at the 1 σ level). Figure 2 also demarcates the eight distinct regions whose fluxes, flux ratios, and relative velocities are tabulated in Table 1.

4 DISCUSSION

4.1 Fluorescent Molecular Hydrogen

The average ratio of the 1 – 0 and 2 – 1 S(1) lines over the whole of P 18 is 2.9 ± 0.4 (Table 1), as expected for fluorescently excited gas slightly modified by a thermal contribution to the v = 1 – 0 S(1) line. Pure fluorescent emission produces a line ratio of ~ 1.7 (e.g., Black & Dalgarno 1976; Black & van Dishoeck 1987), but this ratio can be exceeded when some of the gas is hot enough for the lower levels to be thermalised. We thus conclude, as did Sellgren (1986), that molecular gas in P 18 is irradiated by far-UV photons. It is situated in two arcs around star ‘A’, where some of the gas is hot enough for the v = 1 level to be collisionally populated. This is characteristic of a dense photodissociation region (Sternberg & Dalgarno 1989; BHT). In these PDRs the gas is sufficiently dense that self-shielding

of H_2 occurs for optical depths < 1 from the cloud surface, so that molecules can exist in this warm, primarily atomic region. The typical $1 - 0$ $S(1)$ line flux density in P 18 is $\sim 4 \times 10^{-15}$ ergs cm^{-2} s^{-1} arcsec $^{-2}$, and peaks at 8×10^{-15} ergs cm^{-2} s^{-1} arcsec $^{-2}$ just west of star ‘A’. These fluxes are consistent with the predictions for PDR models for gas of average density, $n \sim 10^4$ cm^{-3} irradiated by far-UV photons from star ‘A’, as we show below.

We estimate the far-UV flux from star ‘A’, a B2–3e star at 1.1 kpc (Sellgren et al. 1996) to be 5060 G_0 in a shell 15'' away. Here $G_0 = 1$ represents the average interstellar radiation field ($= 1.6 \times 10^{-3}$ ergs cm^{-2} s^{-1} ; Habing 1968). For gas of density $\sim 10^4$ cm^{-3} exposed to far-UV fields $G_0 \sim 10^{3-5}$, BHT predict $1 - 0$ $S(1)$ line fluxes of $\sim 3 \times 10^{-15}$ ergs cm^{-2} s^{-1} arcsec $^{-2}$ for a face-on PDR, consistent with the data. Note that our discovery of these arcs, and our interpretation of them as PDRs irradiated by star ‘A’, is at odds with the conclusion of López et al. (1988) that the continuum sources are not stellar, and merely unobscured sight-lines towards a compact H II region. While P 18 shares some of the properties of an H II region, we feel it would be too much of a coincidence if one of these spots also had a location and spectrum consistent with being the excitation source of the PDR.

For such conditions the models predict a purely fluorescent $(1 - 0)/(2 - 1)$ $S(1)$ line ratio of ~ 1.7 , whereas the average ratio for the source is 2.9. This suggests that about half the $1 - 0$ $S(1)$ emission is thermally contributed, and we discuss the implications of this further in § 4.3.

4.2 Geometry and Kinematics

The morphology suggests that star ‘A’ is surrounded by an (incomplete) shell seen in projection, and in this section we investigate whether the distribution of the H_2 line emission is consistent with such a geometry.

Consider a spherical molecular shell surrounding an illuminating star as representing the arc through the N, W, and S peaks. Assuming that the average density in the cloud is low enough so that the emission is mainly fluorescent (see § 4.3), then the H_2 emits primarily from a sheath whose thickness is $A_V \sim 1$, with dust extinction determining the depth to which the far-UV photons penetrate. Viewed from afar the relative intensity along a line of sight is then proportional to the length of the sight line through the shell. We examined models where the thickness of the shell is varied as a proportion of its radius (see Figure 3), and found that when this is $\sim 25\%$ a reasonable fit to the data is achieved. Given the source distance of 1.1 kpc this provides a physical size to the shell, and assuming a standard extinction curve (*i.e.*, $A_V = 1 \equiv N(\text{H}_2) = 2 \times 10^{21}$ cm^{-2}), yields an average density; specifically, for the N, S and W peaks respectively, we obtain thicknesses of $\sim 9, 5,$ and 5×10^{16} cm for the shell and average densities of $\sim 2, 4,$ and 4×10^4 cm^{-3} . The maximum filling factor in this model (ratio of the length of our sight line through the edge of the shell to that if seen face-on) is ~ 3 for a shell thickness $\sim 25\%$ of the radius. These densities are consistent with those derived by applying PDR models to the observed line intensities.

Although the ability of UNSWIRF to resolve lines is limited by its instrumental profile width ($\sim 60 - 70$ km s^{-1} , depending on parallelism), good signal-to-noise data such as

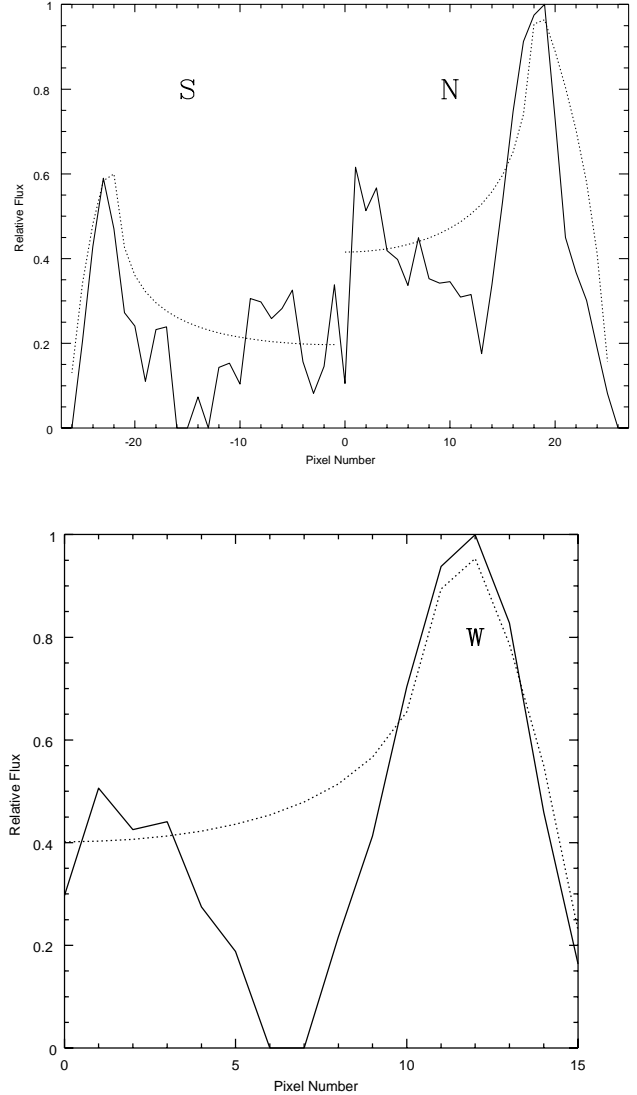


Figure 3. Cuts across the $2.12 \mu\text{m}$ emission in a line (*top*) N–S through star ‘A’, and (*bottom*) E–W through star ‘A’ (solid lines), together with the best fitting model results (dashed lines) for a spherical molecular shell irradiated by star ‘A’ with thickness 25% of the shell radius, where dust extinction limits the region of H_2 excitation to $A_V = 1$. Star ‘A’ is at pixel (0,0) in these plots, with 1 pixel = 1.2×10^{16} cm for a distance to the source of 1.1 kpc.

the $2.12 \mu\text{m}$ observations presented here allow us to measure changes in velocity over the image of only a few km s^{-1} . The velocity data for the $2.12 \mu\text{m}$ line centres (Table 1) show that motions in the gas must be small; differences of at most 10 km s^{-1} are seen between the different regions, with the exception of P 18–NW (Section 4.4).

4.3 Line Ratios

4.3.1 Observed Parameter Space

For a dense PDR, where self-shielding is occurring, H_2 exists at optical depths $A_V < 1$ from the front surface of the cloud. Then, for a sufficiently strong FUV radiation field,

the gas temperature can reach ~ 1000 K or higher, enabling collisions to redistribute the populations in the H_2 energy levels. The $(1-0)/(2-1)$ $S(1)$ line ratio then increases from the pure fluorescent value. It is sensitive to both the density and strength of the FUV field, and so can be used to constrain these parameters in a source. This is different from shock-excited gas where it has been shown empirically that there is little variation in this line ratio both among and within shocked sources (*e.g.*, Burton et al. 1989). In particular, dense clumps of H_2 inside the PDRs may have the $v = 1$ level thermalised, while being surrounded by lower density gas exhibiting pure fluorescent line ratios. Such clumps would signal their presence by elevated levels of the $(1-0)/(2-1)$ $S(1)$ ratio. This could then be used to probe the structure of the clouds.

We have thus sought to determine the fine-structure in the spatial variation of the $(1-0)/(2-1)$ $S(1)$ ratio. We have registered the two images and applied a light Gaussian smooth ($\sigma = 0.3$). In Figure 4 we plot the line ratio so derived against the $(1-0)$ $S(1)$ line intensity. Two sets of symbols are shown in Fig 4; open circles for data points where both the $1-0$ and $2-1$ $S(1)$ lines have $S/N > 3$, and lower limits for pixels where the S/N for the $2-1$ $S(1)$ is < 3 (calculated as though its flux were 3σ). The line ratio rises approximately linearly as the $1-0$ $S(1)$ line flux increases, to a maximum line ratio of ~ 8 , but the dispersion in line ratio increases also. Similar plots for each of the eight distinct regions marked on Figure 2 are presented in Figure 5 (which also illustrates the effect of varying the FUV field) and indicate that most of this spread in line ratio for a given $1-0$ $S(1)$ intensity is intrinsic to regions 2 and 6 (*i.e.*, the northern regions of P 18). Our interpretation of such trends must be guarded however, owing to the large number of lower limits (non-detections in the $2-1$ $S(1)$ line); high ratios for low $1-0$ $S(1)$ fluxes cannot be excluded by our data. Nevertheless, line ratios consistent with pure fluorescence become progressively rarer as the $1-0$ $S(1)$ line flux increases. We now seek to explain the apparent variations in line ratio with emission line flux.

4.3.2 Interpretation

In pure fluorescent gas we would obtain a line ratio of ~ 1.7 , independent of the line intensity. Localised regions of shocked gas would also be evident by a ratio of ~ 10 for a range of line intensities (see Brand et al. 1989). However we see neither such behaviour in P 18 (with the exception of P 18-NW, which we argue in Section 4.4 to be physically unassociated with the other molecular hydrogen emission regions).

Qualitatively the increase in line ratio can be understood as follows. At low density and FUV fields, the $(1-0)/(2-1)$ $S(1)$ ratio is purely fluorescent. However for a fixed FUV field, H_2 of sufficiently high density will be self-shielded, producing a thermal contribution to the $1-0$ $S(1)$ line. Its flux will rise as the density does, while the $2-1$ $S(1)$ line remains purely fluorescent. Thus we expect both the strength of the $1-0$ $S(1)$ line and the ratio with the $2-1$ $S(1)$ line to rise as the density rises.

This line ratio variation can also be understood quantitatively through the PDR models of BHT. BHT derive a number of scaling relations depending on (i) whether n/G_0

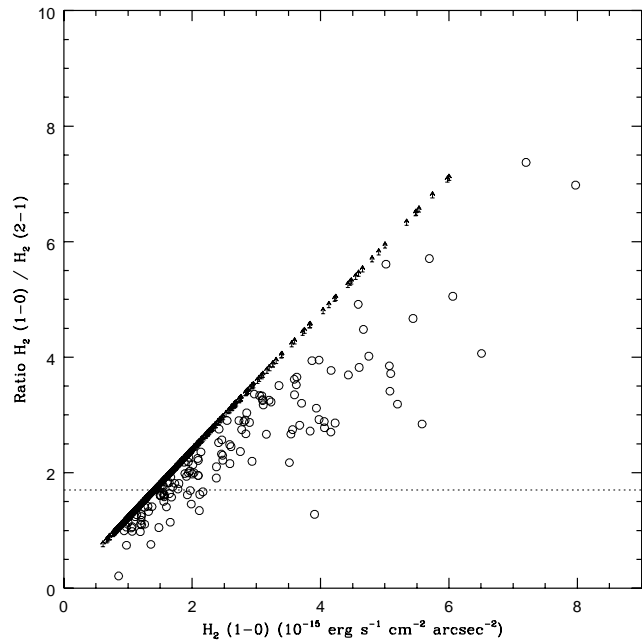


Figure 4. Plot of the H_2 $(1-0)/(2-1)$ $S(1)$ line ratio against $1-0$ line flux in P 18. Open circles are points which have $S/N > 3$ in both lines, while the arrows denote points for which the S/N of the $1-0$ line is > 3 , but the S/N of the $2-1$ line is < 3 ; thus these are lower limits in the ratio. The dashed horizontal line marks a ratio of 1.7, the value expected for purely fluorescent emission. Both images were smoothed by a Gaussian function with $\sigma = 0.3$ before the S/N criterion was applied.

is less than, or greater than 40 cm^{-3} (determining if H_2 self-shielding occurs), and (ii) whether n is less than, or greater than n_{crit} , the density where collisional de-excitation equals the radiative decay rate from a level. The line intensity can be divided into a UV-pumped (I_{pump}) and a thermal (I_{thermal}) part, as follows:

When $n/G_0 \leq 40 \text{ cm}^{-3}$ (self-shielding unimportant):

$$I_{\text{pump}} \propto \begin{cases} n & (n < n_{\text{crit}}) \\ n_{\text{crit}} & (n > n_{\text{crit}}) \end{cases} \quad (1)$$

When $n/G_0 \geq 40 \text{ cm}^{-3}$ (self-shielding important):

$$I_{\text{pump}} \propto \begin{cases} G_0 & (n < n_{\text{crit}}) \\ G_0 n_{\text{crit}}/n & (n > n_{\text{crit}}) \end{cases} \quad (2)$$

The thermal contribution is given by:

$$I_{\text{thermal}} \propto \begin{cases} nN_2\gamma & (n < n_{\text{crit}}) \\ N_2e^{-E/kT}/Z(T) & (n > n_{\text{crit}}) \end{cases} \quad (3)$$

where N_2 is the column of warm H_2 (*i.e.*, at $A_V < 1$) with temperature $\sim T$, E is the energy of the level of interest, γ is the collisional excitation rate from the ground state, and $Z(T)$ is the H_2 partition function.

For the bulk of the gas, with density $n \sim (2-4) \times 10^4 \text{ cm}^{-3}$ and $G_0 \sim 10^{3-4}$, we have both $n < n_{\text{crit}}$ and $n/G_0 < 40 \text{ cm}^{-3}$. The line intensity is then simply proportional to the product of the density and the filling factor, *f*. To within a factor of 3, for $n < 10^5 \text{ cm}^{-3}$, $I_{1-0 S(1)} \sim 3f n_4 \times 10^{-16} \text{ ergs cm}^{-2} \text{ s}^{-1} \text{ arcsec}^{-2}$, where n_4 is the density in units of 10^4 cm^{-3} (see equation 1). As discussed in

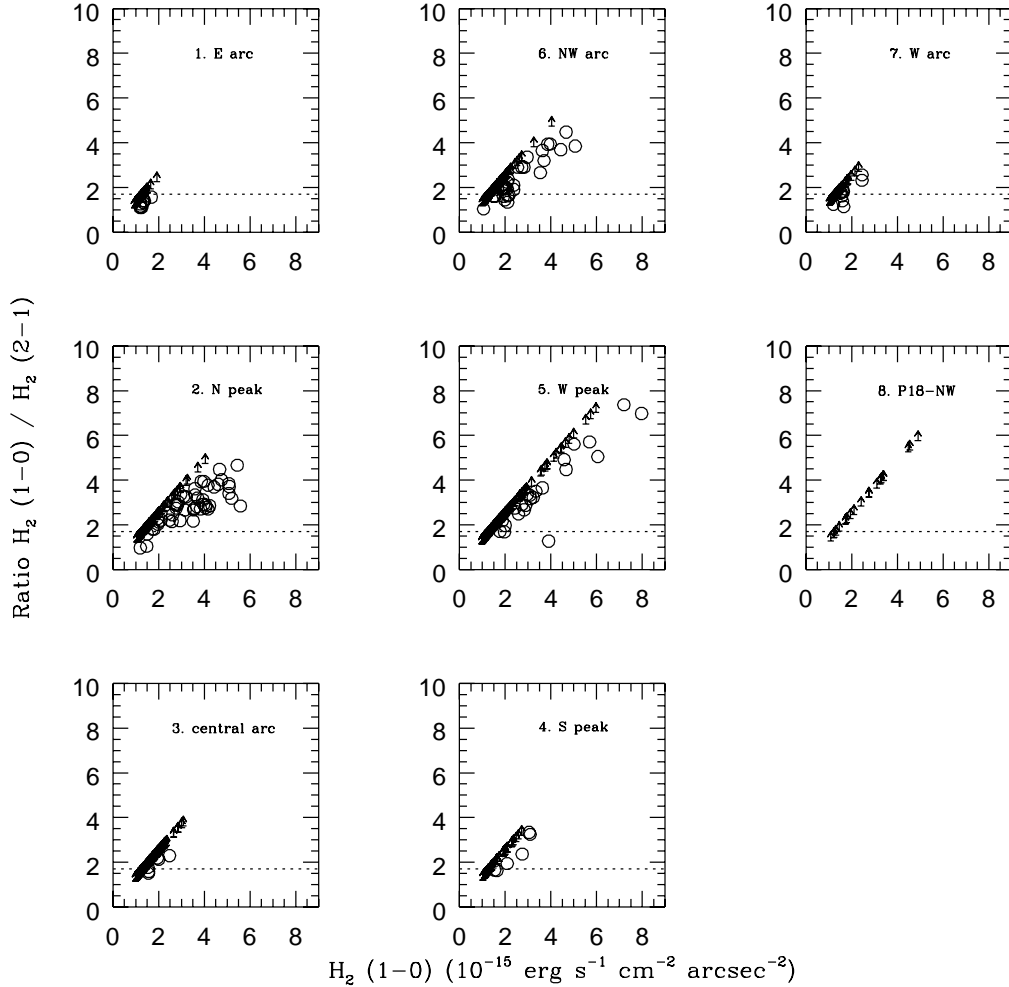


Figure 5. Same as Figure 4, but for the specific regions of P 18 outlined in Figure 2 and listed in Table 1.

§ 4.1, this is consistent with the average line fluxes observed for filling factors of 1–3, with $n_4 = 4$, the value deduced from the geometrical model (see § 4.2).

The detailed models of BHT show that the thermal contribution to the line intensities is negligible when $G_0 = 10^3$, and also when $n \leq 10^5 \text{ cm}^{-3}$ for $G_0 = 10^4$. However for the larger FUV-field, the thermal contribution to the 1–0 $S(1)$ line flux is $\sim 70\%$ for $n = 10^{6-7} \text{ cm}^{-3}$ (the 2–1 $S(1)$ line remains purely fluorescent). Thus higher line fluxes and ratios > 2 imply the presence of some gas of at least this density.

For the E and W arcs (see Table 1), where the G_0 is ~ 2000 , the line ratio is constant at ~ 1.7 . In the N and S peaks and the NW arc, with $G_0 = 5060$, 3500, and 3200 respectively, a thermal contribution to the line ratio is becoming apparent. At the W peak, closest to the illuminating source, where $G_0 = 17800$, both the 1–0 $S(1)$ line intensity and 1–0/2–1 $S(1)$ ratio are highest; the 2–1 $S(1)$ line flux density is however, relatively diffuse at this latter position. On the basis of Figure 5, it would seem reasonable that the Central arc, although apparently superimposed on star ‘A’, must in fact lie at a similar distance from it as the E and W arcs.

These observations can be understood as follows. For the arcs, where the FUV field is low, the emission is purely fluorescent, but the line ratio is insensitive to density. At the N and S peaks, a thermal contribution would be expected for $n \geq 10^6 \text{ cm}^{-3}$. The line ratios at the brightest pixels suggest that $\sim 30\%$ of the 1–0 $S(1)$ emission there is thermal, and thus has densities this high. At the W peak, self-shielding will occur when $n > 40G_0 \sim 5 \times 10^5 \text{ cm}^{-3}$. The data here are thus sensitive to the presence of gas denser than this, a density also larger than n_{crit} . Ratios observed are as high as 7, implying that as much as 70% of the emitting gas at those positions is at least this dense.

Over the W peak, the specific intensity of the 2–1 $S(1)$ line is relatively weaker, in comparison with that of the 1–0 $S(1)$ line, than at the other peaks excited by star ‘A’. In this region, the FUV field G_0 exceeds 10^4 . There is a significant thermal contribution to the 1–0 $S(1)$ flux from dense gas. The 2–1 $S(1)$ flux however remains purely fluorescent. Indeed, as seen by equation 2, its intensity is predicted to decrease as $1/n$, consistent with the observation that it gets relatively weaker. At other peaks, the FUV

field is not sufficiently high for us to expect to observe this behaviour.

The maximum $1 - 0$ $S(1)$ line intensity that is purely fluorescent, arising from gas of average cloud density, occurs when the filling factor is ~ 3 , and the flux density is $\sim 4 \times 10^{-16}$ ergs cm^{-2} s^{-1} arcsec^{-2} for the spherical shell geometry we have modeled. For higher line fluxes a thermal component is present, and the line ratio rises above the pure fluorescent value. The thermal component arises from gas of density at least 10^6 cm^{-3} , and both the highest line fluxes and line ratios occur when the filling factor of this dense gas is greatest.

The spread of observed line ratios between the minimum and maximum values for a fixed $1 - 0$ $S(1)$ line flux can be understood by a variation of the relative filling factors for the low density and high density gas. The lowest ratio occurs when the proportion of low density gas is highest and rises, for a fixed flux level, as both the fraction of low density gas falls and that of the high density gas rises. Thus data with sufficiently high S/N to accurately map the line ratio variation from pixel to pixel could be used to determine the micro-structure of the clumping. The line ratio map (Figure 2), for positions where $G_0 \geq 3000$, is effectively showing the relative amounts of high and low density gas.

We thus conclude that the variations in the line ratio are consistent with the PDR models, self-shielding of gas occurring in its densest parts, with thermal contributions evident when exposed to the highest radiation fields. Localised regions where the density is more than ten times the average exist throughout the molecular cloud. The highest line fluxes and line ratios occur together, where both the filling factor of low and high density gas is greatest, and changes in line ratio from position to position reflect changes in the relative filling factors of these components.

4.4 P 18-NW

The isolated flux peak to the northwest (designated by us as P 18-NW) however, shows no evidence for fluorescent line emission. The $2 - 1$ $S(1)$ line here is barely detected, and the $1 - 0/2 - 1$ $S(1)$ line ratio is clearly thermal in nature, similar to shock-excited values. P 18-NW is too far from star ‘A’ for collisional fluorescence to be significant, as $G_0 < 500$. We suggest that there is a localised source of heating, possibly shocking the gas.

The simultaneous velocity coverage of UNSWIRF offers at least one clue. We notice that the line centre velocity in P 18-NW is also quite different to the rest of P 18. On account of its redshift of $+14$ km s^{-1} relative to the central arc, we speculate that P 18-NW might in fact be associated in some way with the CO outflow source observed by Fukui (1989) and by Felli, Palagi & Tofani (1992). Although Fukui identified the outflow with the position of star ‘A’, the 3 arcmin beam used for the CO observations is much larger than the 45 arcsec separation between star ‘A’ and P 18-NW. The *IRAS* point source discussed by López et al. (1988) and by Felli et al. (1992), namely IRAS 06572 – 0742, has a bolometric luminosity $\sim 1500 L_\odot$ and colours suggestive of an ultra-compact H II region, though neither H_2O (Felli et al. 1992) nor methanol (Walsh et al. 1997) masers have been detected from it. While the *IRAS* positional uncertainties do not preclude an association of P 18-NW with the IRAS

source, it is perhaps more likely that the H_2 line emission observed from P 18-NW is shock-excited by the interaction of an outflow, from an embedded source in P 18, with the ambient cloud material. More detailed CO observations are needed to clarify the influence of any outflow activity on the excitation and environment of P 18.

5 CONCLUSIONS

The reflection nebula Parsamyan 18 has been imaged in both the 2.122 and 2.248 μm emission lines of molecular hydrogen using the UNSW Infrared Fabry-Perot on the AAT, allowing us to study variations in their ratio within the nebula. The emission-line morphology appears as a pair of overlapping arcs, consistent with incomplete PDR shells irradiated by a single early B-type star. We believe we can identify this star in our continuum maps, which contradicts previous claims that the stellar-like sources in P 18 are ‘windows’ in a circumstellar dust shell, illuminated by a compact H II region. Modeling suggests that the thickness of the fluorescing shells is roughly 25% of their radius, with average gas densities of $(2 - 4) \times 10^4$ cm^{-3} , and dust extinction limiting the penetration of the FUV photons. In addition, some regions of P 18 display line ratios indicative of collisional fluorescence in the densest regions exposed to the highest radiation fields. In general, *those regions with the highest intrinsic $1 - 0$ $S(1)$ intensities also have the highest $(1 - 0)/(2 - 1)$ $S(1)$ line ratios*, a result of this process. Within these regions, large ranges in the observed line ratio can be understood as arising from the underlying variations in the relative filling factors of high- and low-density gas. We have discovered an isolated knot of shock-excited H_2 gas just outside the nebula, which we argue on kinematical grounds is more likely to be associated with the CO outflow source reported in this region. This study highlights the advantages of an imaging Fabry-Perot system over traditional long-slit spectroscopy for emission-line imaging, and for understanding the excitation mechanism of molecular hydrogen in particular.

ACKNOWLEDGMENTS

We acknowledge useful discussions with Peter Brand and Antonio Chrysostomou, and suggestions from the referee for improving the paper. We thank Yin-Sheng Sun for valuable assistance in calibrating UNSWIRF. S.D.R. acknowledges the receipt of a UNSW Vice-Chancellor’s Postdoctoral Fellowship. UNSWIRF was funded by a grant from the Australian Research Council.

REFERENCES

- Allen D. A. et al., 1993, PASA, 10, 298
- Black J. H., Dalgarno A., 1976, ApJ, 203, 132
- Black J. H., van Dishoeck E. F., 1987, ApJ, 322, 412
- Brand P. W. J. L., Toner M. P., Geballe T. R., Webster A. S., Williams P.M., Burton M. G., 1989, MNRAS, 236, 929
- Burton M. G., Brand P. W. J. L., Geballe T. R., Webster A. S., 1989, MNRAS, 236, 409
- Burton M. G., Geballe T. R., Brand P. W. J. L., Moorhouse A., 1990, ApJ, 352, 625

- Burton M. G., Hollenbach D. J., Tielens A. G. G. M., 1990, ApJ, 365, 620 (BHT)
- Cohen M., 1974, PASP, 86, 813
- Felli M., Palagi F. Tofani G., 1992, A&A, 255, 293
- Fukui Y., 1989, in *Low Mass Star Formation and Pre-Main Sequence Objects*, ed. B. Reipurth (Garching: ESO), 95
- Gatley I., Hasegawa T., Suzuki H., Garden R., Brand P., Lightfoot J., Glencross W., Okuda H., Nagata T., 1987, ApJ, 318, L73
- Habing H. J., 1968 Bull. Astr. Inst. Netherlands, 19, 421
- Hayashi M., Hasegawa T., Gatley I., Garden R., Kaifu, N., 1985, MNRAS, 215, 31P
- Hilton J., Lahulla J. F., 1995, A&AS, 113, 325
- Hodapp K.-W., 1994, ApJS, 94, 615
- López J. A., Roth M., Friedman S. D., Rodríguez L. F., 1988, Rev. Mexicana Astron. Astrofis., 16, 99
- Ryder S. D., Sun Y.-S., Storey J. W. V., Ashley M. C. B., Burton M. G., Allen L. E., 1997, in preparation
- Sellgren K., 1986, ApJ, 305, 399
- Sellgren K., Werner M. W., Allamandola L. J., 1996, ApJS, 102, 369
- Sternberg A., Dalgarno A., 1989, ApJ, 338, 197
- Stutzki J., Stacey G. J., Genzel R., Graf U. U., Harris A. I., Jaffe D. T., Lugten J. B., Poglitsch A., 1990, in *Submillimetre Astronomy*, eds. G. D. Watt & A. S. Webster (Dordrecht: Kluwer), 269
- Tielens A. G. G. M. Hollenbach D. J., 1985, ApJ, 291, 722
- Walsh A. J., Hyland A. R., Robinson G., Burton M.G., 1997, MNRAS, in press

This paper has been produced using the Royal Astronomical Society/Blackwell Science L^AT_EX style file.